Research Article

optica

Dynamic Transmission Control Based on All-Dielectric Huygens Metasurfaces

AUSTIN HOWES[1], WENYI WANG[2], IVAN KRAVCHENKO[3], JASON VALENTINE[4,*]

[1]*Department of Physics and Astronomy, Vanderbilt University, Nashville, Tennessee 37212, United States*
[2]*Department of Electrical Engineering, Vanderbilt University, Nashville, Tennessee 37212, United States*
[3]*Center for Nanophase Materials Sciences, Oak Ridge National Laboratory, Oak Ridge, Tennessee 37831, United States*
[4]*Department of Mechanical Engineering, Vanderbilt University, Nashville, Tennessee 37212, United States*
**Corresponding author: Jason.g.valentine@vanderbilt.edu*

Received XX Month XXXX; revised XX Month, XXXX; accepted XX Month XXXX; posted XX Month XXXX (Doc. ID XXXXX); published XX Month XXXX

Tunable metasurfaces open new doors for achieving dynamic wavefront manipulation in an ultracompact footprint. Dielectric metasurfaces are particularly attractive for this application due to their low-loss modes. However, their volumetric modes make them difficult to dynamically tune compared to plasmonic variants with strong field confinement. We overcome this challenge by combining dielectric resonators with an ENZ mode in a thin film. By tuning the coupling between modes in the resonators and the ENZ thin film, active control over the transmission amplitude is achieved. Operating at the Huygens wavelength, we demonstrate transmission modulation with an on-state transmission of 70% and a modulation depth of 31%. In addition, we create a tunable diffraction grating and demonstrate its potential use in beam steering applications. This approach provides a new avenue for high speed and low-power modulation of dielectric metasurfaces. © 2018 Optical Society of America

OCIS codes: *(160.3918) Metamaterials; (310.6860) Thin films, optical properties; (310.7005) Transparent conductive coatings; (310.6628) Subwavelength structures, nanostructures.*

http://dx.doi.org/10.1364/optica.99.099999

1. INTRODUCTION

Metasurfaces are planar optical materials formed from arrays of subwavelength resonators [1,2]. The size, shape, and arrangement of the resonators can be used to control the local amplitude, phase, and polarization of an incoming beam, opening new freedoms in wavefront control. This freedom has been used to realize a range of metasurface optics including ultrathin lenses [3,4], waveplates [5,6], and holograms [7-9]. In addition to being much thinner than traditional optical components, metasurfaces can be more sensitive to changes in the dielectric environment due to resonances. This sensitivity can be further amplified by field-concentrating designs. This allows for dynamic tunability using a range of techniques including electrical [10,11], optical [12-14], mechanical [15-18], and phase change-based [19-22] control.

One method to provide this tunability is to integrate plasmonic metasurfaces with active materials. Plasmonic resonances provide large local field enhancement which can be engineered to coincide with an actively tunable material. This allows tuning of the resonator while only changing a small region of the surrounding environment. This is particularly amenable for field effect-based modulation where an extremely small volume is modulated. However, the inclusion of metallic resonators generates unwanted absorption loss. Dielectric resonators are an interesting substitute for plasmonic metasurfaces since they are far less lossy while still exhibiting strong resonances. The main difference between metallic and dielectric metasurfaces is the latter have volumetric modes which naturally result in poorer field confinement. This lack of field confinement makes it more challenging to achieve significant modulation as a large volume of the resonator must be modified.

In this work we present a dynamic dielectric metasurface which operates in transmission at telecom wavelengths. In order to overcome the large mode volume in dielectric resonators, we take advantage of an epsilon-near-zero (ENZ) mode in an electrically tunable ITO layer. ITO is chosen for its convenient plasma wavelength, which can be tuned electrically so that the ENZ point can be located in the spectral region of interest. Operating at the ENZ point provides for large local field enhancement within the ITO leading to dynamic absorption control. Furthermore, we utilize a Huygens mode in the dielectric resonators to minimize impedance mismatch and maximize transmission. This allows for a maximum transmission amplitude of 70% and a modulation depth of 31%.

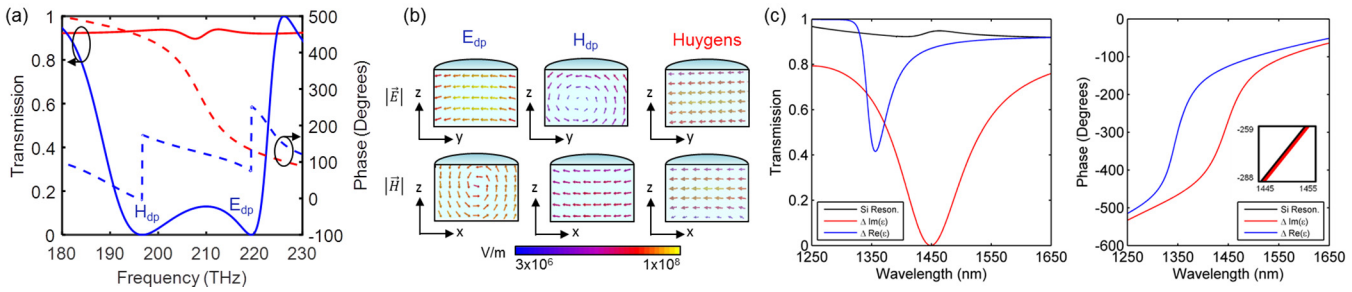

Fig 1: Simulated performance of Si-based metasurfaces with cylindrical particles. (a) Simulated transmission and phase of periodic cylindrical arrays with aspect ratio requirements for the Huygens mode in red. Resonators with an altered aspect ratio are plotted in blue. (b) Planar field vector plots describing the Mie dipole modes present in cylindrical resonator at different frequencies. The first column represents the fields in a cylindrical particle at the electric dipole frequency (labeled in (a)), the second column represents the fields at the magnetic dipole frequency (labeled in (a)), and the third column represents the fields at the Huygens frequency. (c) [Left] Transmission plot of cylindrical resonators upon changing the real and imaginary permittivity of portions of the resonator. The black curve is for Si with a real permittivity of 13.7 and imaginary permittivity of 0. The blue curve has an altered real permittivity of 11.7, and the red curve has an altered imaginary permittivity of 0.7. [Right] Corresponding phase plots for those appearing in [left]. [Inset]: Zoomed plot of the phase data to resolve the two plots.

2. RESULTS

Dielectric resonators possess Mie-type resonances that result in electric and magnetic dipole-like fields at the lowest order modes [23-26]. The spectral position of these resonances depends on the physical dimensions of the particle and the relative locations can be tuned by altering the aspect ratio of the resonator [24]. Figure 1(a) shows the transmission spectrum of two arrays of Si cylinders. Silicon is chosen for near-IR Mie-resonant metasurfaces due to its high refractive index and low loss. The two dips in the blue transmission curve correspond to the magnetic and electric field Mie dipole modes, each of which accumulate a phase change of π. Figure 1(b) shows field vector plots for the Si resonators at the frequencies of each Mie resonance. Changing the aspect ratio of the particle results in spectral movement and eventual overlap of the magnetic and electric dipole resonances as shown with the red curve. When this occurs with two dipole modes of equal strength, the reflected fields from one dipole mode are out of phase with those of the other, resulting in perfect transmission [27-30]. In addition, the phase accumulation of the two resonances is combined, creating a smooth 2π phase gradient across the resonance resulting in what is known as a Huygens mode [27-30]. Figure 1(b) verifies that at the Huygens mode wavelength (λ_H) there exists both an electric and magnetic dipole field profile within the resonator.

Huygens surfaces provide a convenient route for achieving perfect transmission using dielectric metasurfaces. For dynamic control, this response can be modified by changing the index of the resonator to disrupt the Huygens mode. Figure 1(c) demonstrates the effect of modifying the real and imaginary parts of the index of a cylindrical dielectric particle. If we modify the real permittivity from 13.7 to 11.7, individual dipole resonances again appear in the transmission spectrum since the Huygens criteria is not satisfied, resulting in an altered spectra and phase response. If we instead modify the imaginary permittivity from 0 to 0.7, the phase profile is unaffected but the transmission is suppressed at the Huygens mode wavelength due to absorption. In real devices, actively changing the index of an entire metasurface structure to this degree is challenging. While phase change materials can possess permittivity changes of this magnitude, they often also exhibit large absorption losses. Instead, we investigate if we can produce similar effects by changing the index of a small fraction of the resonator.

In order to achieve significant modulation, we take advantage of the ENZ point in an adjacent film [31]. Various studies involving ENZ modes have provided unique methods for spontaneous emission enhancement [32], optical switching [33], and cloaking [34]. The primary benefit of utilizing an ENZ mode for modulation is that one can achieve enhanced fields in the ENZ medium. This is possible due to the continuity of the normal displacement field across the interface between two media ($\varepsilon_{1,n}E_{1,n} = \varepsilon_{2,n}E_{2,n}$). As the permittivity of a material drops to zero, the fields within it will increase, providing stronger modal overlap. Transparent conductive oxides such as indium tin oxide (ITO) are well-suited for this task when working in the near-infrared as they support large doping levels. The integration of ITO as an active component with a silicon resonator supporting a Huygens resonance mode is shown in Figure 2(a). Figure 2(b) depicts the permittivity of ITO as a function of its plasma wavelength. By changing the local carrier concentration, the wavelength at which the real permittivity crosses 0 can be controlled. Importantly, the Huygens mode has strong E_z near the top of the cylindrical resonator due to the circulating electric field in the magnetic dipole mode, as shown in figure 1(b). If the Huygens wavelength (λ_H) is spectrally overlapped with the ENZ mode of the ITO layer, then the z-oriented electric field in the ITO will be dramatically enhanced due to continuity of the z-oriented displacement field. Figure 2(c) displays the z-oriented electric field density within the resonators. These plots are based on an accumulation layer thickness of 3 nm [35-37] and are generated from full-wave simulations using CST Microwave Studio. Field enhancement in the ITO is observed when the ENZ point of ITO coincides with the Huygens wavelength of the resonators, as shown in Fig. 2(c). Similarly, if the ENZ mode of the ITO is tuned away from the Huygens wavelength (λ_H), then the field enhancement disappears. Since the imaginary component of ITO's permittivity is finite at the ENZ point, tuning through this point results in tunable absorption as shown in figure 2(d). This is accompanied by a reduction in transmission

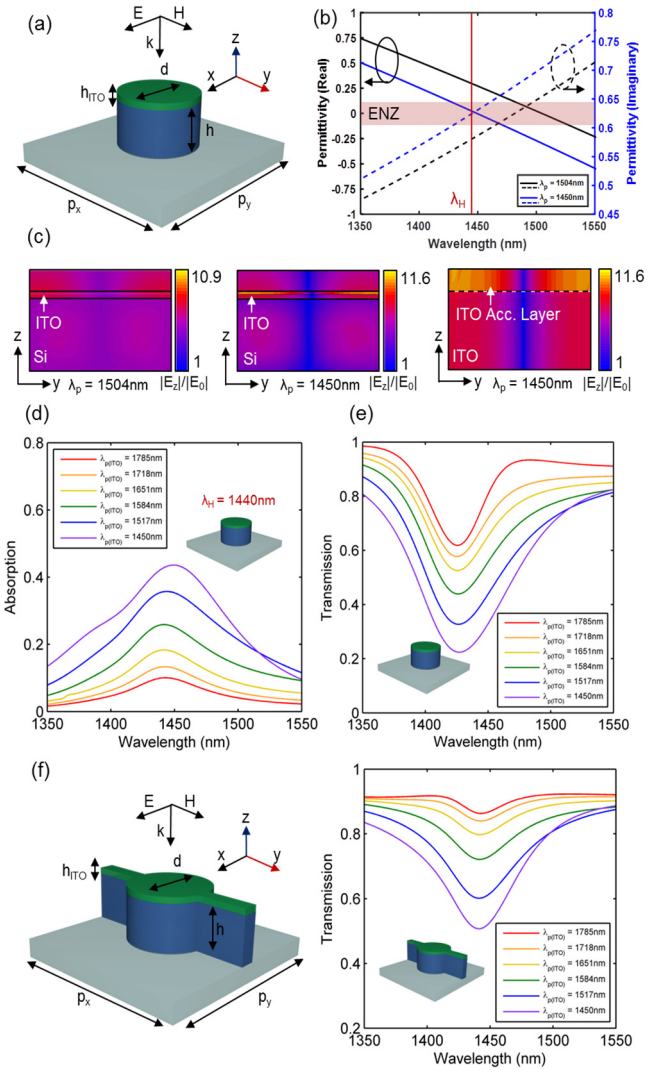

Fig 2: (a) Unit cell schematic for a silicon Huygens metasurface with an integrated ITO film on top. $p_x = p_y = 800$nm, $h = 230$nm, $h_{ITO} = 10$nm, and $d = 480$nm. (b) Real and Imaginary ITO permittivity as a function of wavelength. The red line intersecting with the x-axis indicates the Huygens wavelength for the silicon resonator. The red bar intersecting with the y-axis indicates the ENZ mode range for ITO. (c) E_z field profiles for the resonator depicted in (a). The left and center figures contain ITO with plasma frequency spectrally separated and overlapped with the Huygens wavelength, respectively. The right figure is a zoomed in field profile of the ITO when its plasma frequency is overlapped with the Huygens wavelength. The estimated carrier concentration in the accumulation layer and remainder of ITO is 8.6e20 e^-/cm^3 and 3.56e20 e^-/cm^3, respectively. (d) Simulated absorption for the metasurface in (a) for several plasma wavelengths, increasing as the plasma wavelength approaches the Huygens wavelength. (e) Simulated transmission for the same metasurface. (f) Unit cell schematic including dielectric bars for electrically connecting the ITO across resonators. The bar width is 80nm. [Right] Simulated transmission spectrum for the metasurface including bars.

(figure 2(e)) resulting in a modulation depth of 41% at λ_p= 1450 nm.

In order to modify the local carrier concentration of multiple cylindrical resonators in an array, they need to be electrically connected. To accomplish this, we introduce thin bars in our unit cell structure, seen in figure 2(f). This does not greatly impact the simulated performance for light with magnetic field polarized along the bar axis (Figure 2(g)), since the resonator dimensions crucial for the magnetic dipole resonance are not affected by adding the bars. The performance for light with electric field polarized along the bar axis is presented in Supplementary Figure 1. Though the off-state transmission is higher for the architecture with connected resonators, the modulation depth remains at 40% due to higher transmission in the on-state. To experimentally realize these devices, we constructed a Si metasurface array integrated with a thin active ITO modulation layer with Au contacts and a solid electrolyte top gate. The schematic is illustrated in figure 3(a). Quartz wafers with an amorphous silicon layer on top were first treated with a Boron dopant and annealed in a tube furnace to increase conductivity. After thorough HF cleaning, the Si array was patterned by creating a Cr etch mask using electron beam lithography (EBL) followed by deposition and lift-off (see Methods section for details). Reactive ion etching (RIE) was used to define the Si resonators. After removing the Cr mask, we performed two rounds of optical lithography, deposition, and lift-off to define the ITO and Au layers respectively. After the first round of lithography, we annealed the device in a tube furnace to move the plasma frequency of ITO near the Huygens wavelength of the resonators. Finally, a solid electrolyte solution was applied to the top of the sample to serve as the electrostatic gate for actively tuning the plasma frequency of ITO.

Figure 3(c) illustrates the working principle of the device. One electrode is attached to the ITO, and the other is connected to the electrolyte. By applying a bias voltage between the solid electrolyte and the ITO, a charge bilayer forms at the interface between the two materials. This causes the local carrier density to increase in the charge accumulation region of the ITO, which modulates the local permittivity and therefore the spectral position of the ENZ mode.

Experimental transmission data is plotted in Figure 4(a) for a device with a Huygens wavelength of 1470nm. The transmission is modulated between 0.71 and 0.42 as we change the bias voltage between +10V and -10V. Note that a bias voltage of 0V does not result in maximum transmission as the Huygens mode is near the plasma wavelength of the unbiased ITO. Applying a negative bias moves the ITO plasma wavelength closer to the Huygens wavelength, decreasing transmission, whereas applying a positive bias moves the ITO plasma wavelength farther from the Huygens wavelength, increasing transmission. The simulated transmission spectra of the device are shown in Figure 4(b). The Huygens mode should exist at 1450nm with a transmission modulation of 0.8 to 0.35. The difference in Huygens frequency between simulated and experimental data can be attributed to the fact that fabrication techniques limit our accuracy in defining the height of the silicon resonators. Figure 4(c) is a series of images in an IR camera of our sample illuminated with 1470nm light fed through a monochrometer. As we change the bias voltage, the array appears darker, indicative of the lower transmission. Figure 4(d) shows the change in transmission is gradual for intermediate voltages. To ensure modulation is not due to a change in the electrolyte, a control sample with no ITO was fabricated and demonstrated no change in transmission. (See Supplementary Figure 2). This is also verified by the fact that the bus bar lines remain transmissive in Figure 4c when biasing the sample. The

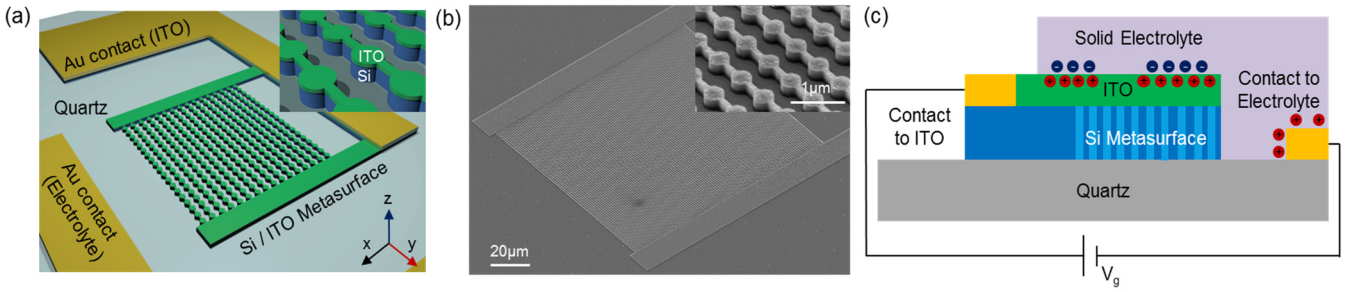

Fig 3: (a) 3D Cartoon of the fabricated device. The bias voltage is applied between the Electrolyte contact and the ITO contact. [Inset] Zoomed image of the resonator structure within the array. (b) SEM Images of the fabricated Si array. (c) Cartoon demonstrating the working principle of the device. The electric bilayer formed at the Solid Electrolyte / ITO interface is responsible for the local increase in ITO carrier density, changing its permittivity.

average switching speed was found to be 88s and is dictated by the carrier mobility of the solid electrolyte. Since the carrier density of ITO is modulated via a field effect, the time response of this device can be greatly improved using a more traditional metal / oxide gate.

By selectively patterning ITO over particular regions of the Si array, we can make select areas absorptive while the rest of the array remains highly transmissive. This freedom enables not only tunable filtering as seen in Figure 4, but also reversible diffraction-based beam steering. To demonstrate this effect, we designed and fabricated a device in which alternating strips of the ITO are electrically connected. The device schematic is outlined in Figure 5(a-b). Upon positive bias the electrically connected regions will be become transmissive resulting in uniform transmission across the array and a single output beam. Imaging the sample in the Fourier plane, as shown in Figure 5(c), confirms that one output beam is observed for this bias condition. The dotted circle represents the numerical aperture of the objective. The electrically connected strips will become absorbing upon negative bias, resulting in a diffraction pattern with beam maxima dictated by $psin\theta = m\lambda$, where p=8um, λ=1470nm, and m is the diffracted order. Figure 5(d) demonstrates the experimental performance of the device under negative bias. We indeed observe the zero, first, and second order diffracted modes in the Fourier plane. The simulated intensity plots on the right indicate the expected angular position of the diffracted modes for a grating with period p=8um, which coincide with the experimental images. This device serves as a proof of concept for reversibly modulating these ultrathin structures and could easily be expanded to more complicated designs.

In summary, we have presented a method to locally modify volumetric Mie resonances using the ENZ point of thin conductive oxides. By choosing to utilize dielectric resonators we avoid the absorption losses inherent to metallic devices and operate in transmission instead of reflection. For these reasons, this approach offers a unique solution for compact spatial light modulators and dynamic optics in the near-infrared region. To realize a switching speed which is compatible with these applications the architecture can be improved by replacing the electrolyte with a more traditional metal and dielectric gate.

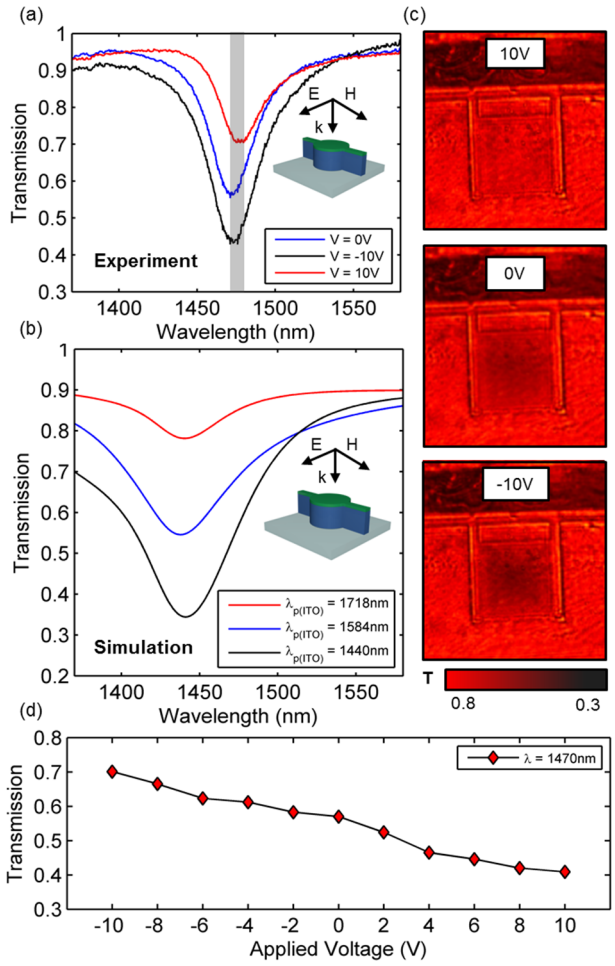

Fig 4: Transmission experiment results. (a) Experimental transmission spectrum of the fabricated device at three distinct applied bias voltages. (b) Simulated transmission spectrum of the fabricated device at three distinct ITO plasma wavelengths. The grey vertical bar indicates the wavelength at which IR camera images in (c) were taken. (c) IR Camera images of the device at three bias voltages using monochromatic light at the working wavelength of the device. (d) Peak transmission amplitude as a function of bias voltage, showing several intermediate voltage steps.

3. METHODS

LPCVD silicon on quartz wafers were fabricated at Oak Ridge National Laboratory after which a Boron dopant (B-153 Filmtronics, Inc.) was applied via spincoating at 4000rpm. The sample was then baked on a hot plate at 200°C for 20 mins. We annealed the sample in a tube furnace at 1010°C for 45 min, then exposed to O_2 gas at 850°C for 10 mins to oxidize the top Si layer. Afterwards, the device was washed in a 10% HF:DI-H_2O solution to remove the oxide. We removed the

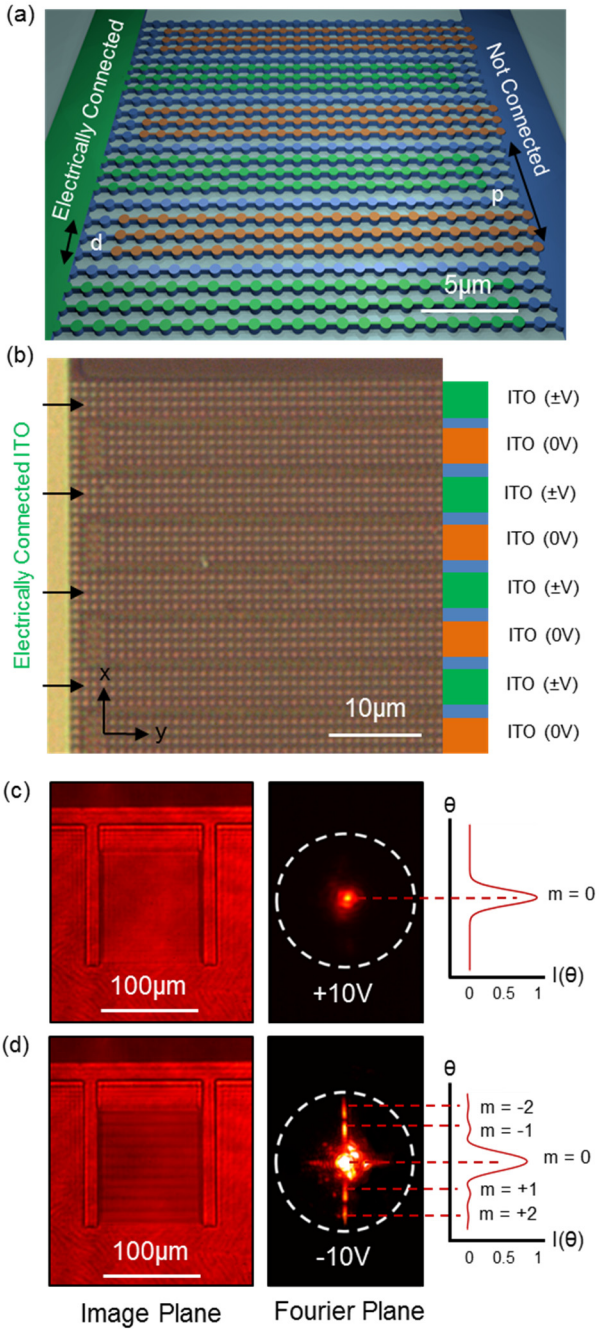

Fig 5: (a) Cartoon of the ITO grating structure over the array with dimensions d = 3.2um and p = 8um. Horizontal strips of ITO cover the array, which alternate between those connected to an electrode and those not electrically connected. (b) Optical Image of the completed device with patterned ITO in bars across the resonator array. [Right] Colored schematic illustrating which portions of the array are electrically modulated. The colors match with those illustrated in (a). (c) [Left] IR Camera image at 1470nm light of the device at a positive bias voltage. [Right] Fourier plane image after an aperture was restricted to the metasurface array. The white dashed circle represents the maximum angular field of view due to the numerical aperture of the objective used in the experiment (26°). (d) [Left] IR Camera image at 1470nm light of the device at a negative bias voltage. [Right] Fourier plane image showing the diffraction pattern of the device. The plots on the right are simulated intensity plots of the diffraction pattern, labeled with the expected modes for a grating with period p = 8um (m=±1, 10.6°) (m=±2, 21.4°).

back-side Si by spincoating a protective photoresist layer on the front side and performing RIE. After removing the photoresist, the front side Si thickness was measured using spectroscopic ellipsometry. If the height was above the resonator target height, we used oxidation to convert some of the Si to SiO_2, which was then removed with HF.

Afterwards, we performed EBL and development (using A4 PMMA as the photosensitive film and 1:3 MIBK:IPA as the developing agent) to define the Si pattern. We deposited a 35nm Cr layer to function as an etch mask and lifted off the PMMA with PG Remover. The Si resonators were defined using RIE to etch through the remaining Si, and the device was cleaned with an O_2 plasma treatment.

We again spincoated photoresist on the device (6000rpm) and baked it for 2 min at 95°C. After exposing the ITO layer design in the photoresist using optical lithography, developing in MK-319 (Dow Inc.), and cleaning the sample again with O_2 plasma treatment, we deposited a 10nm ITO layer using RF sputtering. The sample was annealed to modify the ITO plasma frequency, which was verified using spectroscopic ellipsometry. Once the photoresist was removed via liftoff in acetone, we repeated this process to define the Au electrode layer, using thermal evaporation as the deposition mechanism.

Finally, a solid electrolyte solution was prepared to serve as the electrostatic gate. We used a bi-(trifluoromethylsylfonyl) amine lithium salt dissolved in poly (ethylene oxide)[38] in order to index match the electrolyte and SiO_2 substrate to minimize reflection from the interface. This was prepared by mixing 0.05 Li salt, 0.3g poly(ethylene oxide), and 20ml of acetonitrile at 90 deg. C for 5 mins, then centrifuging the solution at 6000rpm for 15 mins and pipetting the tops of the resultant fluid into separate airtight vials. After soldering wires onto the device electrodes, we applied electrolyte to the device by spincoating at 800rpm and baking the sample at 90°C for 5 mins.

Funding. National Science Foundation (NSF) (ECCS-1351334); Office of Naval Research (ONR) (N00014-16-1-2283).

Acknowledgment. A portion of this research was conducted at the Center for Nanophase Materials Sciences, which is sponsored at Oak Ridge National Laboratory by the Scientific User Facilities Division, Office of Basic Energy Sciences, U.S. Department of Energy.

See Supplement 1 for supporting content.

REFERENCES

1. N. Yu, P. Genevet, M. Kats, F. Aieta, J. Tetienne, F. Capasso, Z. Gaburro, "Light propagation with phase discontinuities: Generalized laws of reflection and refraction," Science, 334, no. 333 (2011).
2. X. Ni, N.K. Emani, A.V. Kildishev, A. Boltasseva, V.M. Shalaev, "Broadband Light Bending with Plasmonic Nanoantennas," Science, 335, p. 427 (2012).
3. F. Aieta, P. Genevet, M. Kats, N. Yu, R. Blanchard, Z. Gaburro, F. Capasso, "Aberration-Free Ultrathin Flat Lenses and Axicons at Telecom Wavelengths Based on Plasmonic Metasurfaces," Nano Letters, 12, no. 4932 (2012).
4. A. Arbabi, Y. Horie, A. Ball, M. Bagheri, A. Faraon, "Subwavelength-thick Lenses with High Numerical Apertures and Large Efficiency Based on High Contrast Transmitarrays," Nature Communications, 6, No. 7069 (2015).
5. N. Yu, F. Aeita, P. Genevet, M. Kats, Z. Gaburro, F. Capasso, "A Broadband, Background-Free Quarter-Wave Plate Based on Plasmonic Metasurfaces," Nano Letters, 12, No. 12, pp. 6328-6333 (2012).

6. Y. Yang, W. Wang, P. Moitra, I. Kravchenko, D. Briggs and J. Valentine, "Dielectric meta-reflectarray for broadband polarization conversion and optical vortex generation", Nano Letters, 4, no. 1394 (2014).
7. Ni, X., Kildishev, A. V. & Shalaev, "V. M. Metasurface holograms for visible light," Nature Communications, 4, no. 2807 (2013).
8. Lin, J., Genevet, P., Kats, M. A., Antoniou, N. & Capasso, "F. Nanostructured holograms for broadband manipulation of vector beams," Nano Letters, 13, pp. 4269–4274 (2013).
9. L. Huang, X. Chen, H. Mühlenbernd, H. Zhang, S. Chen, B. Bai, Q. Tan, G. Jin, K. Cheah, C. Qiu, J. Li, T. Zentgraf, S. Zhang, "Three-dimensional optical holography using a plasmonic metasurface," Nature Communications, 4, no. 2808 (2013).
10. Y. Huang, H. Lee, R. Sokhoyan, R. Pala, K. Thyagarajan, S. Han, D. Tsai, H. Atwater, "Gate-Tunable Conducting Oxide Metasurfaces," Nano Letters, 16, no. 9, pp.5319-5325 (2016).
11. Y. Yao, R. Shankar, M. Kats, Y. Song, J. Kong, M. Loncar, F. Capasso, "Electrically Tunable Metasurface Perfect Absorbers for Ultrathin Mid-Infrared Optical Modulators," Nano Letters, 14, no. 11, pp. 6526-6532 (2014).
12. M. Shcherbakov, S. Liu, V. Zubyuk, A. Vaskin, P. Vabishchevich, G. Keeler, T. Pertsch, T. Dolgova, I. Staude, I. Brener, A. Fedyanin, "Ultrafast all-optical tuning of direct-gap semiconductor metasurfaces," Nature Communications, 8 (2017).
13. M. Shcherbakov, P. Vabishchevich, A. Shorokhov, K. Chong, D. Choi, I. Staude, A. Miroshnichenko, D. Neshev, A. Fedyanin, Y. Kivshar, "Ultrafast all-optical switching with magnetic resonances in nonlinear dielectric nanostructures," Nano Letters, 15, p. 6985 (2015).
14. Y. Yang, W. Wang, A. Boulesbaa, I. I. Kravchenko, D. P. Briggs, A. Puretzky, D. Geohegan, J. Valentine "Nonlinear Fano-Resonant Dielectric Metasurfaces", Nano Letters, 15, p. 7388 (2015).
15. H. Ee, R. Agarwal, "Tunable Metasurface and Flat Optical Zoom Lens on a Stretchable Substrate," Nano Letters, 16, no. 4, pp. 2818-2823 (2016).
16. J. Y. Ou, E. Plum, J. Zhang, N. Zheludev, "An electromechanically reconfigurable plasmonic metamaterial operating in the near-infrared," Nature Nanotechnology, 8, p.252-255 (2013).
17. P. Gutruf, C. Zou, W. Withayachumnankul, M. Bhaskaran, S. Sriram, C. Fumeaux,"Mechanically Tunable Dielectric Resonator Metasurfaces at Visible Frequencies," Nano Letters, 10, no. 1, pp.133-141 (2015).
18. I. Pryve, K. Aydin, Y. Kelaita, R. Briggs, H. Atwater, "Highly Strained Compliant Optical Metamaterials with Large Frequency Tunability," Nano Letters, 10, p. 4222-4227 (2010).
19. Z. Zhu, P. Evans, R. Haglund, J. Valentine, "Dynamically Reconfigurable Metadevice Employing Nanostructured Phase-Change Materials," Nano Letters, 17, no. 8, pp.4881-4885 (2017).
20. Q. Wang, E. Rogers, B. Gholipour, C. Wang, G. Yuan, J. Teng, N. Zheludev, "Optically reconfigurable metasurfaces and photonic devices based on phase change materials," Nature Photonics, 10, p. 60-65 (2016).
21. B. Gholiqour, J. Zhang, K. MacDonald, D. Hewak, N. Zheludev, "An all-optical, non-volatile, bidirectional, phase-change meta-switch," Adv. Materials, 25, p. 2050-3054 (2013).
22. L. Liu, L. Kang, T. Mayer, D. Werner, "Hybrid metamaterials for electrically triggered multifunctional control," Nature Communications, 7, no. 13236 (2016).
23. A. Evlyukhin, S. Novikov, U. Zyweitz, R. Eriksen, C. Reinhardt, S. Bozhevolnyi, B. Chichkov, "Demonstration of Magnetic Dipole Resonances of Dielectric Nanospheres in the Visible Region," Nano Letters, 12, No. 7, p. 3749-3755 (2012).
24. I. Staude, A. E. Miroshnichenko, M. Decker, N. T. Fofang, S. Liu, E. Gonzales, J. Dominguez, T. S. Luk, D. N. Neshev, I. Brener, and Y. Kivshar, "Tailoring Directional Scattering through Magnetic and Electric Resonances in Subwavelength Silicon Nanodisks," ACS Nano, 7, pp. 7824-7832 (2013).
25. A. Kuznetsov, A. Miroshnichenko, Y. H. Su, J. Zhang, B. Luk'yanchuk, "Magnetic Light," Scientific Reports, 2, no. 492 (2012).
26. J. Schuller, M. Brongersma, "General properties of dielectric optical antennas," Opt. Express, 17, p.24084-24095 (2009).
27. F. Monticone, N. Estakhri, A. Alù, "Full Control of Nanoscale Optical Transmission with a Composite Metascreen," Physical Review Letters, 110, No. 203903 (2013).
28. C. Pfeiffer, A. Grbic, "Metamaterial Huygens' Surfaces: Tailoring Wave Fronts with Reflectionless Sheets," Physical Review Letters, 110, no. 197401 (2013).
29. C. Pheiffer, N. Emani, A. Shaltout, A. Boltasseva, V. Shalaev, A. Grbic, "Efficient light bending with isotropic metamaterial Huygens' surfaces," Nano Letters, 14, p.2491-2497 (2014).
30. M. Decker, I. Staude, M. Falkner, J. Dominguez, D. Neshev, I. Brener, T. Pertsch, Y. Kivshar, "High-Efficiency Dielectric Huygens Surfaces," Adv. Opt. Mater., 3, No. 6, pp.813-820 (2015).
31. M. Silveirinha, N. Engheta, "Tunneling of Electromagnetic Energy through Subwavelength Channels and Bends using ε-Near-Zero Materials," Physical Review Letters, 97, No. 157403 (2006).
32. Y. Lu, R. Sokhoyan, W. Cheng, G. Shirmanesh, A. Davoyan, R. Pala, K. Thyagarajan, H. Atwater, "Dynamically controlled Purcell enhancement of visible spontaneous emission in a gated plasmonic heterostructure," Nature Communications, 8, no. 1631 (2017).
33. D. de Ceglia, S. Campione, M. A. Vincenti, F. Capolino, and M. Scalora, Low-damping epsilon-near-zero slabs: Nonlinear and nonlocal optical properties, Phys. Rev. B, 87, 155140 (2013).
34. A. Alù, M. Silveirinha, A. Salandrino, N. Engheta, "Epsilon-near-zero metamaterials and electromagnetic sources: Tailoring the radiation phase pattern," Phys. Rev. B, 75, p. 115410 (2007).
35. S. Zhu, G. Q. Lo, D. L. Kwong, "Design of an ultra-compact electro-absorption modulator comprised of a deposited TiN/HfO2/ITO/Cu stack for CMOS backend integration," Optics Express, 22, Issue 15, pp. 17930-17947 (2014).
36. M. Kwon, "Discussion of Two Ways of Optically Modeling Indium-Tin-Oxide Layers in Slot Waveguides for Waveguide Analysis," IEEE Photonics Journal, 8, no.1 (2016).
37. E. Feigenbaum, K. Diest, H. A. Atwater, "Unity-order index change in transparent conducting oxides at visible frequencies," Nano Letters, 10, no. 10, p. 2111-2116 (2010).
38. D. Prasai, A. Klots, A. Newaz, J. S. Niezgoda, N. Orfield, C. Escobar, A. Wynn, A. Efimov, G. K. Jennings, S. J. Rosenthal, and K. Bolotin, "Electrical control of near-field energy transfer between quantum dots and 2D semiconductors," Nano Letters, 15, no. 7, pp. 4347–4380 (2015).